

The role of the proteins Kar9 and Myo2 in orienting the mitotic spindle of budding yeast

Dale L. Beach, Julie Thibodeaux, Paul Maddox, Elaine Yeh and Kerry Bloom

Background: Two genetic 'pathways' contribute to the fidelity of nuclear segregation during the process of budding in the yeast *Saccharomyces cerevisiae*. An early pathway, involving Kar9p and other proteins, orients the mitotic spindle along the mother–bud axis. Upon the onset of anaphase, cytoplasmic dynein provides the motive force for nuclear movement into the bud. Loss of either pathway results in nuclear-migration defects; loss of both is lethal. Here, to visualize the functional steps leading to correct spindle orientation along the mother–bud axis, we imaged live yeast cells expressing Kar9p and dynein as green fluorescent protein fusions.

Results: Transport of Kar9p into the bud was found to require the myosin Myo2p. Kar9p interacted with microtubules through the microtubule-binding protein Bim1p and facilitated microtubule penetration into the bud. Once microtubules entered the bud, Kar9p provided a platform for microtubule capture at the bud cortex. Kar9p was also observed at sites of microtubule shortening in the bud, suggesting that Kar9p couples microtubule shortening to nuclear migration.

Conclusions: Thus, Kar9p provides a key link between the actin cytoskeleton and microtubules early in the cell cycle. A cooperative mechanism between Kar9p and Myo2p facilitates the pre-anaphase orientation of the spindle. Later, Kar9p couples microtubule disassembly with nuclear migration.

Background

During the process of budding in the yeast *Saccharomyces cerevisiae*, the mitotic spindle aligns with the mother–bud axis to correctly distribute the duplicated genomes. The determinants of spindle polarity (reviewed in [1]) include dynein (Dhc1p) and dynactin components, kinesins (Kip3p), microtubule-binding proteins (Bim1p/Yeb1p) and cell-polarity markers (Kar9p, Bni1p/She5p and Bud6p/Aip3p). Dynein is synthetically lethal with *bni1/she5*, *bud6/aip3* and *kar9* [2–4], defining two primary pathways that establish spindle orientation. The 'early' pathway orients the spindle with respect to the mother–bud axis and proximity to the bud neck, while the 'late' pathway coincides with anaphase onset to translocate the daughter nucleus into the bud. Mutations in one pathway are compensated by the other; mutations in both are lethal. For instance, both *kar9* and dynein mutations generate binucleate cells [5–7], but the double mutant is temperature sensitive or lethal [2,4,8].

Originally identified as a karyogamy mutant, *kar9* was later found to affect nuclear position during mitosis [5,9]. A small population of binucleate cells occurs in the absence of Kar9p. Kar9p is localized specifically at the bud tip in vegetative cells, and to the tip of the mating projection in cells induced to enter the mating pathway [5].

Address: Department of Biology, University of North Carolina, 212 Coker Hall CB3280, Chapel Hill, North Carolina 27599-3280, USA.

Correspondence: Kerry Bloom
E-mail: Kerry_Bloom@unc.edu

Received: 12 May 2000
Revised: 25 October 2000
Accepted: 25 October 2000

Published: 15 November 2000

Current Biology 2000, 10:1497–1506

0960-9822/00/\$ – see front matter

© 2000 Elsevier Science Ltd. All rights reserved.

Although Bni1p and Bud6p are required to maintain Kar9p at the bud cortex [3], both Bni1p and Bud6p also affect bipolar bud-site selection and actin polarity [10–12]. A role for actin in spindle orientation has been described [13–17], but the interaction between the actin and microtubule cytoskeletons remains unknown.

Specific actin alleles and mutations of actin-associated proteins produce off-axis spindles as well as binucleate cells [15–17]. Actin cables and not actin patches [18] are required at the inception of the cell cycle to correctly orient the spindle [14]. Transport of polarity determinants along actin cables may be the key requirement for actin function early in the cell cycle. Type V myosins and actin cables are required for transport of a variety of components into the bud [19–21]. Ash1p is a cell-fate determinant whose localization is specified in part by the polar distribution of the mRNA transcript [22,23]. *ASH1* mRNA localization to the bud tip is dependent on Bni1p and Bud6p [22–25]. Of the five genes originally described for the localization of the Ash1p (*SHE1–SHE5*), *SHE1* is a class V myosin (*MYO4*), and *SHE5* is *BNI1* [26]. Subsequent investigation identified an *ASH1* mRNA anchorage defect for *bud6* similar to *bni1/she5* [24]. In the absence of either protein, *ASH1* mRNA is released from a tight association with the bud tip and moves throughout the bud. Thus,

Bni1p and Bud6p provide positional cues for spindle orientation and contribute to asymmetric mRNA localization.

KAR9 is one of the few spindle-polarity determinants that does not exhibit such pleiotropic phenotypes. In the absence of Kar9p, the nucleus fails to congress to the bud neck or the mating projection [3,5]. The *kar9* cells exhibit nuclear migration phenotypes similar to *kip3*, *bim1/yeb1*, *bni1/she5* and *bud6/aip3* [3,8,27–30]. However, mutations in *kip3*, *bim1/yeb1*, *bni1/she5* and *bud6/aip3* have additional phenotypes that exacerbate nuclear migration, such as altered microtubule dynamics (*bim1/yeb1* and *kip3* [27,28,31]) or diminished actin integrity (*bni1/she5* and *bud6/aip3*). Kar9p interacts biochemically with the microtubule plus-end binding protein Bim1p [31–33], and requires actin, Bni1p and Bud6p to maintain a cortical attachment within the bud [3,5]. Here, by imaging live yeast cells expressing Kar9p as a green fluorescent protein fusion (Kar9–GFP), we observed the dynamic cortical and microtubule localization of Kar9p and the facilitated orientation of the microtubule towards the incipient bud site. Kar9p transport into the bud was dependent on *MYO2* [34], which encodes a class V myosin, and a polarized actin cytoskeleton. We also observed Kar9p at sites of microtubule shortening in the bud, indicating Kar9p to be a key component of the mechanism that couples microtubule shortening to nuclear migration.

Results

Kar9p is not required for *ASH1* mRNA localization

To determine whether Kar9p also contributes to *ASH1* mRNA anchorage, we observed the localization of *ASH1* mRNA in *kar9Δ* cells (KBY1010). Direct observation of the mRNA in live cells is possible through ‘green RNA’ (gRNA) techniques using an RNA-binding protein found in the bacteriophage MS2 [24,25]. In *kar9Δ* cells, gRNA_{ASH1} localization in vegetative and mating cells was indistinguishable from that in wild-type cells; gRNA_{ASH1} appeared as a fluorescent spot within 0.3 μm of the bud tip during bud growth ($n = 10$; Figure 1a–d, both cells), then migrated to the neck approximately 20 minutes before cell separation ($n = 4$; Figure 1a–d, right cell). Finally, gRNA_{ASH1} became localized at the incipient bud site prior to bud initiation without leaving the cell cortex (data not shown). In the mating pathway, the gRNA_{ASH1} spot was positioned at the mating projection tip where the spot retained dynamic activity in both α-factor arrested ($n = 10$; data not shown) and mating *kar9Δ* cells ($n = 5$; data not shown).

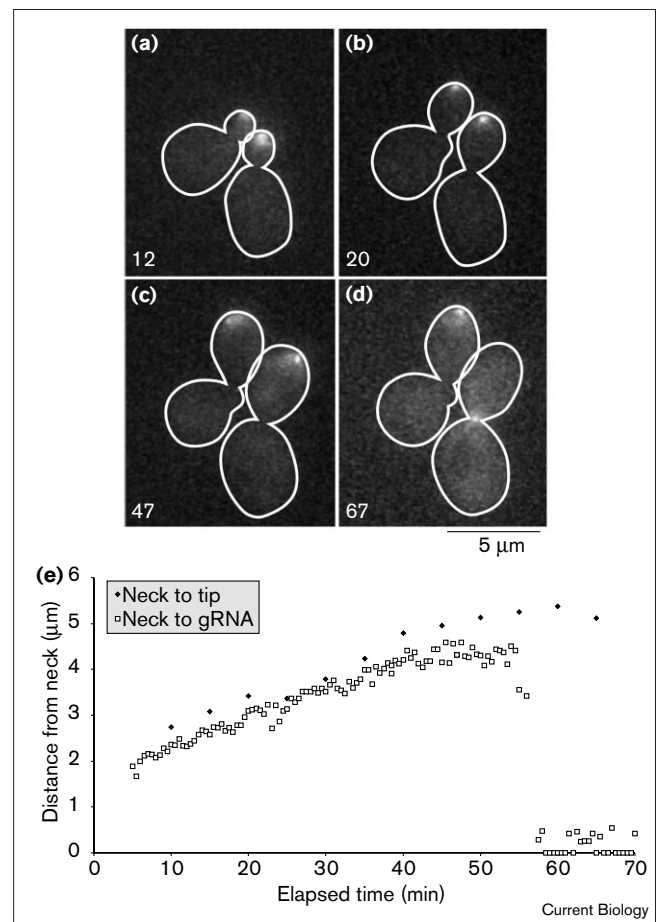
The temporal relation between bud growth and gRNA_{ASH1} position is demonstrated graphically in Figure 1e. The graph shows that in the *kar9Δ* cell gRNA_{ASH1} is associated with the bud tip, as has been observed for gRNA_{ASH1} in wild-type cells [24]. Migration of gRNA_{ASH1} to the neck is illustrated by the precipitous drop at 55 minutes (Figure 1e). Maintenance of gRNA_{ASH1} localization at sites

of polarized growth during both vegetative and mating periods of the life cycle in *kar9Δ* cells indicates that Kar9p is not required for *ASH1* mRNA anchorage.

Kar9p is mobile within the bud and co-localizes with cytoplasmic microtubules

A Kar9–GFP fusion protein expressed under the control of the *MET25* promoter rescued the nuclear-position defect in a *kar9Δ* strain (KBY1010). Binucleate cells were not detected in KBY1010 cells expressing Kar9–GFP ($n = 300$),

Figure 1



Localization of *ASH1* mRNA is independent of Kar9p. (a–d) *ASH1* mRNA localization as visualized by gRNA_{ASH1} expression [24] in *kar9Δ* cells (KBY1010). In both cells shown, gRNA_{ASH1} was localized at the bud tip throughout bud growth. In (d), gRNA_{ASH1} became localized to the neck in the cell on the right. The white outlines were traced from differential interference contrast (DIC) images and transposed onto the correlating fluorescent image to define the cell outline. Elapsed time (min) is shown at the bottom left. (e) The distance from the neck to the bud tip, and from the neck to the gRNA_{ASH1} spot, was measured for both cells. Only the plot for the right cell is shown. The distances of the bud tip and the gRNA_{ASH1} spot from the neck were within 0.3 μm, demonstrating that gRNA_{ASH1} remains associated with the bud tip throughout the cell cycle; gRNA_{ASH1} returned to the neck after ~55 min. See Supplementary movie 1.

Table 1**Kar9-GFP localization.**

											<i>n</i>
	a	b	c	d	e	f	g	h	i	j	<i>n</i>
Wild type	21.0	36.0	4.0	20.0	10.5	0.0	1.5	3.0	1.5	1.5	132
Integrand	22.0	32.0	0.5	38.0	1.6	0.5	0.5	4.1	0.0	1.1	187
Wild type + Lat-A	28.6	5.4	4.3	5.4	5.7	11.6	0.6	13.4	21.3	3.6	164
<i>bni1Δ</i>	17.7	6.1	6.1	4.7	1.9	0.0	0.0	17.8	11.2	34.6	214
<i>bud6Δ</i>	17.9	9.0	12.1	8.5	7.6	0.0	0.0	17.0	0.9	28.3	223
<i>bim1Δ</i>	11.3	62.4	3.4	16.0	4.0	2.6	0.0	0.4	0.0	0.0	532
Azide + dGlu	13.5	11.5	0.0	10.6	7.7	2.4	0.0	10.2	22.1	19.2	208
Wild type + Nz	31.7	42.7	5.7	8.4	7.5	0.9	0.0	2.2	0.0	0.9	227
<i>bni1Δ</i> + Nz	18.0	0.0	12.0	43.0	15.0	12.0	0.0	0.0	0.0	0.0	194

The table shows the percentage of each cell population with the indicated pattern of Kar9-GFP localization (columns a–j). All cell types listed expressed a Kar9-GFP fusion protein from a CEN plasmid via the *MET25* promoter, except 'Integrand', where the GFP coding region

was fused to the endogenous *KAR9* chromosomal locus (see Materials and methods). Lat-A, latrunculin-A; azide + dGlu, sodium azide and deoxyglucose; Nz, nocodazole.

compared with 11% ($n = 309$) in untransformed *kar9Δ* cells. Additionally, Kar9-GFP expression from the *MET25* promoter did not produce any binucleate cells after a 2 hour induction ($n = 300$), and the nucleus was properly positioned within the mother cell prior to anaphase onset ($n = 300$). An integrated Kar9-GFP fusion protein expressed from the endogenous promoter maintained similar localization (Table 1).

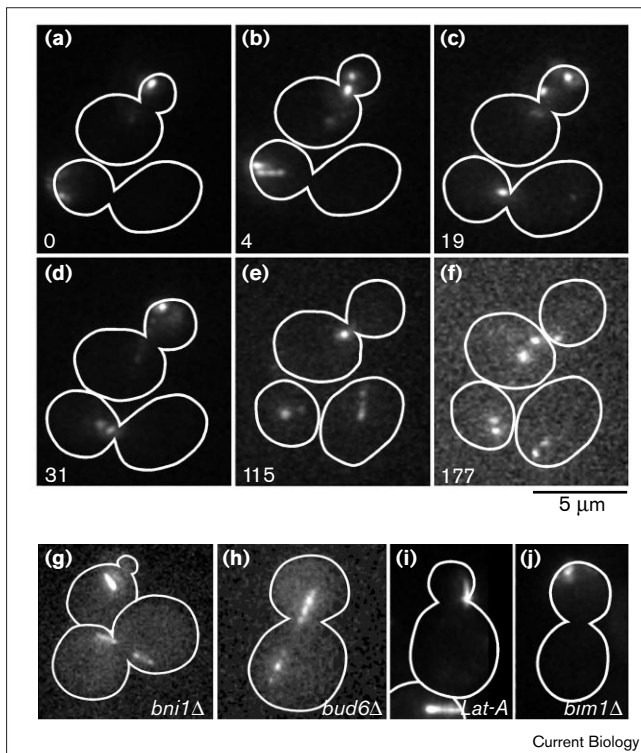
Kar9-GFP, expressed in wild-type cells (YEF473A) from the *MET25* promoter, was observed as cortical spots (Figure 2a,c,d) and either punctate or continuous linear arrays (Figure 2b,e; see also Table 1g–j). Typically, 1–2 cortical spots were observed within each cell, and each remained mobile within the bud during growth. Spots moved with an average velocity of $1.96 \pm 1.24 \mu\text{m}/\text{minute}$ ($n = 10$) within the bud. This velocity is rapid when compared with the average velocities of Bud6-GFP ($0.116 \mu\text{m}/\text{minute}$) and gRNA_{ASH1} ($0.31 \mu\text{m}/\text{minute}$) [24], yet very slow in comparison with actin patch movements ($16.8 \mu\text{m}/\text{minute}$) [35]. Cortical Kar9-GFP movements were diffusional, as cortical spots remained motile in the presence of sodium azide and deoxyglucose, which inhibit ATP production (see below and Table 1) [36]. The Kar9-GFP cortical spots migrated to the neck 30 ± 10 minutes ($n = 6$) prior to cell separation (Figure 2c, lower cell; Figure 2e, upper cell; Table 1d). Approximately 20 minutes ($n = 4$) after the Kar9-GFP became localized to the neck, it was released from the cortex and observed as spots and/or filaments within the cytoplasm (Figure 2e, lower cell; Figure 2f, upper cell). Unlike *ASH1* mRNA, Kar9p-GFP became cytoplasmic, as spots and linear arrays, before being localized to the bud site. Prior to the next budding cycle, Kar9-GFP linear arrays oriented towards the incipient bud site 13 ± 4 minutes ($n = 7$) before bud emergence (see below).

Kar9-GFP linear arrays depended on microtubules, as evidenced by their absence upon nocodazole treatment (Table 1). Microtubules can be imaged by either decorating the filament with a dynein-GFP fusion protein [37] or by labeling the tubulin directly (GFP-Tub1) [38]. Line scans of microtubules (see Materials and methods) differentiated periodic Kar9-GFP spots from continuous dynein-GFP decoration along microtubules. While Kar9-GFP appeared as discrete peaks of fluorescent intensity along the filament, microtubules labeled by dynein-GFP displayed linear fluorescence as did GFP-Tub1 [38] or Tub3-GFP (K.B., unpublished data). Dynamic growth ($0.808 \pm 0.426 \mu\text{m}/\text{minute}$; $n = 35$) and shortening ($0.574 \pm 0.253 \mu\text{m}/\text{minute}$; $n = 39$) of Kar9-GFP linear arrays coincided with microtubule dynamics measured in an isogenic strain containing dynein-GFP ($0.798 \pm 0.29 \mu\text{m}/\text{minute}$ growth, $n = 12$; $0.791 \pm 0.347 \mu\text{m}/\text{minute}$ shortening, $n = 19$) and in *kar9Δ* cells containing dynein-GFP ($0.703 \pm 0.416 \mu\text{m}/\text{minute}$ growth, $n = 17$; $0.630 \pm 0.325 \mu\text{m}/\text{minute}$ shortening; $n = 16$). Therefore, microtubule dynamics in *kar9Δ* cells and cells expressing Kar9-GFP are not significantly different from the wild type.

Kar9p preferentially localizes along microtubules in the absence of cortical anchors

The dynamic movement of Kar9-GFP between cortical spots and microtubules is indicative of the bipartite distribution of Kar9p. Cells treated with latrunculin-A (to depolymerize actin filaments) or deleted for *BNI1/SHE5* or *BUD6/AIP3* showed a loss of Kar9-GFP spots from the bud cortex and an increase in microtubule-associated Kar9-GFP (Figure 2g–i; Table 1); *bni1Δ/she5Δ* cells had an 83% decrease in Kar9p spots at the bud cortex; *bud6Δ/aip3Δ* cells decreased cortical Kar9-GFP by 75%. Latrunculin-A-treated cells decreased cortical Kar9-GFP

Figure 2



Kar9-GFP is localized to the bud cortex and microtubules in wild-type cells. Kar9-GFP localization in (a–f) wild-type cells, (g) *bni1Δ* mutants, (h) *bud6Δ* mutants, (i) latrunculin-A-treated wild-type cells (YEF473A), and (j) *bim1Δ* mutants. (a) Medium budded cell (top) and a large budded cell (bottom), each with a spot of Kar9-GFP at the cell cortex. Examination of optical sections taken through the cell distinguished cortical versus cytoplasmic positioning of the Kar9-GFP spot. (b) Both cells contain linear arrays of GFP fluorescence. The top cell contains two spots along a line (note elongation of the spot within the neck), while the lower cell contains a punctate (lower) and continuous (upper) array. (c) The top cell contains two separated spots that are not associated with an array. In the lower cell, the Kar9-GFP spot has returned to the neck. (d) The top cell contains a Kar9-GFP spot in the bud, and a faint linear filament extending into the mother cytoplasm. The lower cell contains two spots adjacent to the neck, and will undergo cell separation within 5 min (not shown). (e) Kar9-GFP has moved to the neck of the top cell. The bottom cell has completed cell separation, and the Kar9-GFP is seen as cytoplasmic spots in the daughter (left) and as a punctate linear array in the mother (right). (f) Both cells have completed cell separation, and Kar9-GFP is cytoplasmic in the unbudded cells. Elapsed time (min) is shown at the bottom left of each panel. In this and subsequent figures, the white borders outline the cell surface. See Supplementary movies 2–5.

by 85% (Table 1b). Wild-type cells treated with sodium azide and deoxyglucose [36] had a 68% decrease in cells with cortical spots in the bud (Table 1b), suggesting that cortical localization of Kar9p depends on ATP. Disruption of actin filaments resulted in an 11-fold increase in cells containing labeled microtubules observed within mother cells (Figure 2i), as well as the appearance of cortical spots within the mother in 11.6% of the population (Table 1f).

Increased microtubule labeling was also observed in *bni1/she5* and *bud6/aip3* strains, and ATP-depleted cells (Table 1i–j).

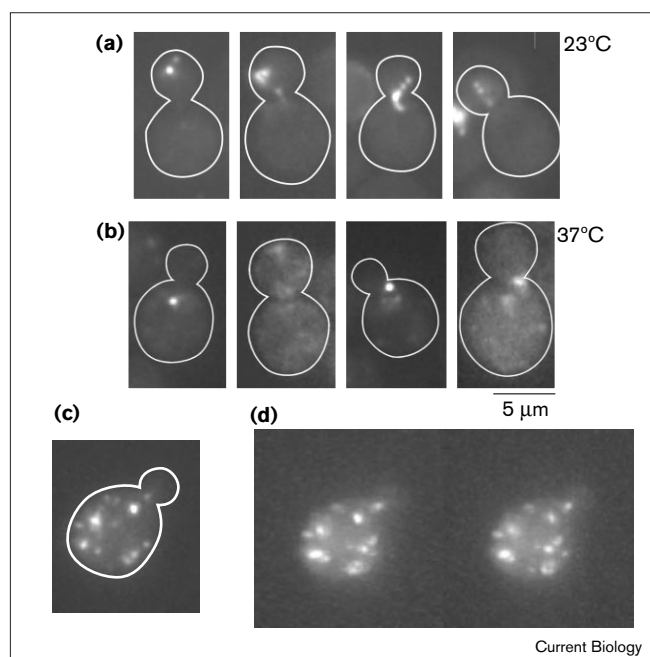
In the absence of the Bni1p/She5p and Bud6p/Aip3p cortical anchors, Kar9p relocated from the bud cortex to microtubules in both mother and bud. In contrast, Kar9-GFP remained localized to the bud cortex in cells deleted for *BIM1/YEB1* (Table 1), confirming that Kar9p association with microtubules requires Bim1p/Yeb1p [32,33,39]. Thus, Kar9p is resident at two discrete structures: the bud cortex and the microtubule.

Kar9p is delivered to the bud through Myo2p

Bud6p/Aip3p and *ASH1* mRNA require, respectively, *MYO2* and *MYO4/SHE1*, for proper localization [21–26,40]. Kar9p localized properly and retained motility within the bud in the absence of microtubules (Table 1 and data not shown), indicative of a microtubule-independent delivery mechanism. To determine whether either of the known yeast class V myosins transports Kar9p between mother and bud, we observed the localization of Kar9-GFP in *myo4* and *myo2* mutant strains. Kar9-GFP localization appeared wild type in a *myo4/she1* deletion strain (data not shown), but was disrupted in the *myo2-66* temperature-sensitive strain [41]. After a 5 minute shift to the restrictive temperature (37°C), Kar9-GFP in a *myo2-66* strain was distributed throughout mother and bud in 34% ($n = 98$) of the population as diffuse patches (Figure 3b) or punctate spots (Figure 3c,d). At the restrictive temperature, 22% ($n = 98$) of cells contained Kar9-GFP only in the mother in contrast to 10% ($n = 244$) for cells at the permissive temperature (see Figure 3). Only 9% of the wild-type cells (YEF473A) had a punctate distribution of Kar9-GFP throughout the cell at 37°C ($n = 54$). As wild-type cells maintain Kar9p predominantly within the bud, the redistribution of Kar9-GFP between both mother and bud demonstrated a significant effect upon loss of Myo2p. These data indicate that the elevated temperature specifically affects a Myo2p-dependent process, and establishes a role for Myo2p in the asymmetric localization of Kar9p. Recent biochemical results indicate a direct interaction between the Myo2p tail and Kar9p [34].

Myo2-dependent transport occurs along actin cables

Recovery of filamentous actin after latrunculin-A treatments [42] allowed us to observe actin-based Kar9p transport into the bud. As the *bim1Δ/yeb1Δ* strain precluded Kar9p deposition on microtubules (Table 1), treatment of *bim1Δ/yeb1Δ* cells with latrunculin-A generated cortical spots of Kar9-GFP in both mother and bud (compare Figure 2i with Figure 4). When latrunculin-A was removed from the cultures, motile Kar9-GFP spots moved towards the bud at an average velocity of $1.52 \pm 1.03 \mu\text{m}/\text{second}$, peaking at $4.09 \mu\text{m}/\text{second}$ ($n = 5$; Figure 4). The Kar9-GFP migration rates are likely to represent a minimal velocity

Figure 3

MYO2, which encodes a class V myosin, is required for Kar9p localization in the bud. **(a,b)** Selected images of individual *myo2-66* cells expressing Kar9–GFP at 23°C (a) when held at 23°C or (b) transferred to 37°C for 5 min before imaging. **(c)** A *myo2-66* cell with punctate Kar9–GFP distribution at the permissive temperature (23°C), then shifted to the restrictive temperature (37°C) for 5 min. **(d)** Stereo images of a three-dimensional reconstruction (see Materials and methods) of the cell shown in (c). Large spots were visible along the cortex, and smaller spots could be seen in the cytoplasm.

for Kar9p transport, as cells must re-establish a polarized actin cytoskeleton following exposure to latrunculin-A during image acquisition. Kar9p particles halted at the neck for approximately 1–10 seconds before continuing into the bud ($n = 5$; note the spot at the neck in Figure 4d). By generating a Kymograph (see Materials and methods) for a linear region corresponding to the path of a Kar9–GFP spot (Figure 4a–d), a second particle was detected following the same route in approaching the bud neck (Figure 4e,f). Therefore, Kar9p particles are transported to the bud neck via Myo2p along ‘tracks’ within the mother. These tracks may be actin cables within the mother, polarized towards the bud [25,42–45].

Temperature-sensitive alleles of tropomyosin specifically lose filamentous actin at the restrictive temperature [19]. To determine the role of actin cables in localizing Kar9p, we imaged Kar9–GFP in *tmp1-2*, *tpm2Δ* cells (ABY971) at both the restrictive (35°C) and permissive (22°C) temperature. Transport of Kar9–GFP into the bud was greatly diminished in the absence of actin cables (22.4% in the mother cell at 35°C, $n = 85$; 3.2% in the mother cell at 22°C, $n = 94$). The large fraction of cells with Kar9p in the

body of the mother cell in *tmp1-2*, *tpm2Δ* cells illustrates the requirement for filamentous actin in Kar9p transport to the bud.

Kar9p facilitates microtubule search and capture at the bud site

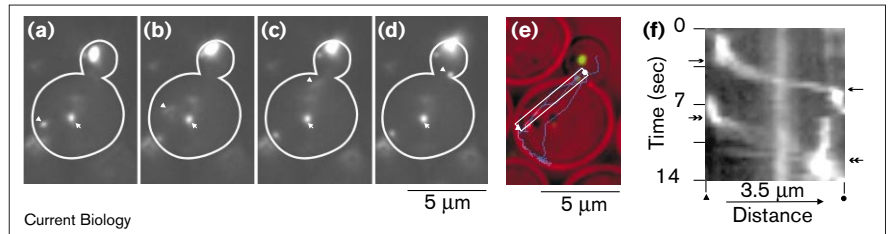
Microtubules probe the cell cortex in a ‘search and capture’ mechanism prior to finding the bud, and, reportedly, bind cortical-attachment sites associated with the actin cytoskeleton [37,46–50]. Kar9p is present prior to bud emergence as evidenced by the persistence of Kar9–GFP produced from the endogenous promoter (Table 1a). As Kar9p is delivered early to the neck via actin and myosin, and associates with microtubules via Bim1p/Yeb1p, Kar9p may provide the critical link between the microtubule and actin cytoskeletons.

Cells were observed between cell separation and initial microtubule penetration of the bud in the presence and absence of Kar9p. Where the direction of the bud is defined as 0°, and perpendicular to the mother–bud axis is 90°, microtubules in *kar9Δ* cells emanated from the spindle pole body (SPB) at $72.3^\circ \pm 54.4^\circ$ ($n = 9$) from the mother–bud axis at the time of bud emergence. In contrast, wild-type microtubules were within $43.1^\circ \pm 29.8^\circ$ ($n = 7$) [27]. Microtubules in the wild-type strain (YEF473A) intersected, and remained associated with the pre-bud site 8.7 ± 11.7 minutes ($n = 10$) prior to bud emergence, while in the *kar9Δ* strain (KBY1010) microtubules entered the bud 36.8 ± 18.3 minutes ($n = 7$) after bud emergence. The timing of microtubule entry into the bud in the *kar9Δ* strain was remarkably similar to the timing of nuclear migration to the neck in a *bim1Δ/yeb1Δ* strain (36.7 minutes) [51]. Thus, microtubules in *kar9Δ* cells were delayed in finding the bud site by 45.5 minutes (8.7 minutes prior + 36.8 minutes post). This delay may contribute to the frequency of binucleate cells found in *kar9Δ* strains. Six of 12 *kar9Δ* cells constructed the mitotic spindle before microtubules detected the bud, while microtubules entered the bud prior to spindle formation in 10 of 10 wild-type cells.

To determine whether Kar9p facilitates microtubule penetration of the bud, we observed Kar9–GFP early in the cell cycle. The microtubule decorated by Kar9–GFP in Figure 5a extended into the cytoplasm of the cell approximately 30° off the mother–bud axis (cell separation followed in 34 minutes; Figure 5d). The Kar9–GFP-labeled microtubule contacted the cell cortex (Figure 5b,g), prior to localization at the incipient bud site (Figure 5c), and continued to migrate towards the incipient bud site ($n = 5$). Once the microtubule reached the bud site, Kar9–GFP was concentrated at that site (Figure 5c; $n = 3$). The microtubule remained associated with the bud site, then immediately entered the emergent bud (Figure 5d; $n = 7$).

Figure 4

Kar9p is transported along actin filaments within the mother towards the bud. (a–d) Following a 15 min treatment with 50 μ M latrunculin-A, *bim1 Δ /yeb1 Δ* (KBY1017) cells expressing Kar9–GFP were allowed to recover, and the movements of Kar9–GFP spots were imaged at 3 frames per second. (a) Two spots were labeled within the mother domain of the cell (arrowhead and arrow). (b–d) While the central spot (arrow) remained stationary, the left spot (arrowhead) migrated towards the neck. (d) The motile spot remained adjacent to the neck (10 sec for this spot). Elapsed time (in sec) is shown corresponding to the time scale in (f). (e) A composite of a bright-field image (red), an epifluorescent image of GFP signal (green), and traces generated by the 'Track Points' function of Metamorph (see Materials and methods) of Kar9–GFP particles through the cell (blue). Kar9–GFP within the bud is apparent, while the traces show the path



followed by Kar9–GFP towards the bud. The rectangular region was used to form the Kymograph (see Materials and methods). (f) The Kymograph function extracts a user-defined region (rectangle in panel e) of an image to be displayed with sequential time points colinear within a single image. Elapsed time is represented along the vertical axis (sec), and distance (μ m) along the horizontal axis (oriented to the image in panel e by the triangle and circle). The vertical, off-center trace is the non-motile spot in the middle of

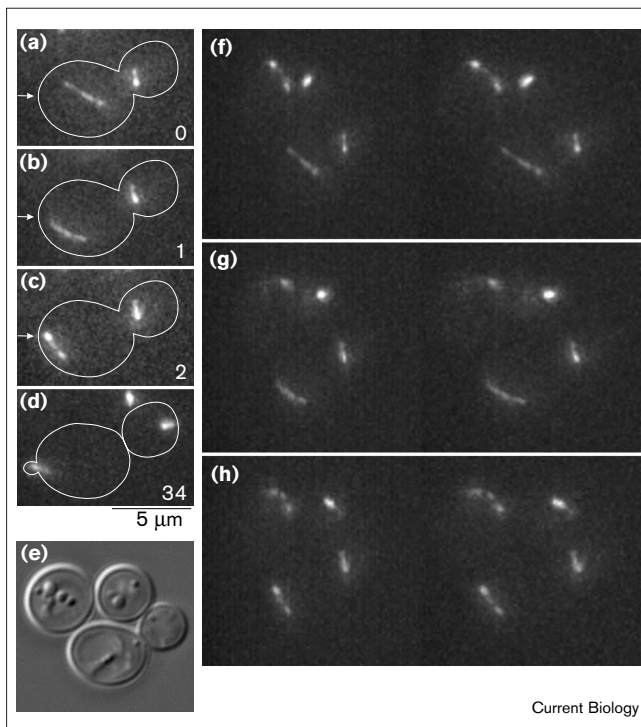
the cell. Single- and double-headed arrows mark the beginning and end of two sigmoid-shaped traces of motile Kar9–GFP spots being translocated from the mother towards the bud neck. The top trace is the same spot indicated by the arrowhead in (a–d) and within the rectangle in (e), and the lower trace is a second spot following the same path (indicated by the arrow in panels a,c,d). Vertical regions of each sigmoidal trace indicate stationary periods. See Supplementary movie 6.

Kar9p couples microtubule dynamics with nuclear migration

To examine the relation between Kar9p within the bud and microtubules, we coexpressed both Kar9–GFP and dynein–GFP. Microtubules, visualized by dynein–GFP labeling, were observed extending into the bud and contacting Kar9–GFP spots. The Kar9p–microtubule intersections were unstable, lasting an average of 2.36 minutes ($n = 5$), similar to previous reports of the persistence of microtubule–cortex interactions [37]. Microtubule–Kar9p

cortical spot interactions were visible as the intersection of linear, filamentous microtubules with fluorescent spots at the cortex (see Figure 6c,e,f), and occurred $54\% \pm 9.5$ ($n = 6$) of the time, on average, throughout the cell cycle.

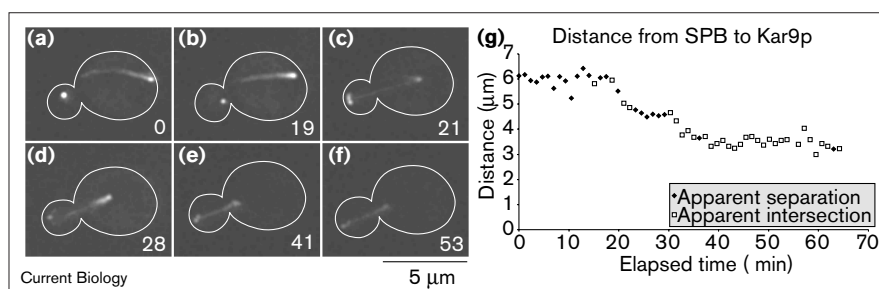
Kar9p–microtubule contacts facilitated the orientation and positioning of the nucleus at the bud neck (Figure 6). Kar9–GFP was localized as a spot in the bud, and a microtubule growing from the SPB (bright spot distant from the neck) extended towards the bud (Figure 6a). Once the microtubule bundle entered the bud and connected with the Kar9p spot (at the tip of the bud in Figure 6a–c), the nucleus (marked by the SPB) moved towards and, ultimately, adjacent to the neck (Figure 6c–f). Microtubules shortened as the nucleus traveled towards the neck at an average velocity of $0.404 \pm 0.153 \mu\text{m}/\text{minute}$ ($n = 5$). Migration of the nucleus towards the neck arrested when

**Figure 5**

Kar9p facilitates microtubule delivery to the bud site. (a–c) Sequential images of a Kar9–GFP-labeled microtubule and (f–h) the respective stereo images of three-dimensional renderings (see Materials and methods). The incipient bud site is labeled by an arrow in (a–c). Bipolar budding in this haploid strain (YEF473A) is occasionally observed. (a) A large budded, post mitotic cell with Kar9–GFP-labeled microtubules in both mother and daughter cells. The asterisk marks the SPB. The plus-end of the microtubule is oriented towards the incipient bud site. (b) Microtubule movement to contact the cell cortex. Inspection of the optical sections (not shown) and (g) three-dimensional stereo view demonstrated cortical attachment of the microtubule. (c) The microtubule plus-end was positioned at the incipient bud site 32 min prior to cell separation. (d) The new bud is visible, and a microtubule decorated by Kar9–GFP has penetrated the small bud. (e) DIC image of the three cells shown in the stereo images. The large budded cell is represented in (a–c). Elapsed time (min) is shown.

Figure 6

Kar9p couples dynamic microtubules with nuclear migration. **(a–f)** Selected time-lapse images of a cell expressing both Kar9–GFP (spot in bud) and dynein–GFP (decorates the microtubule and SPB in the mother). The SPB is the bright spot at the right end of the microtubule. **(a,b)** The Kar9–GFP spot is mobile within the bud. The microtubule in the mother domain is oriented with the plus-end towards the bud, scanning the bud cortex to locate the bud site. **(c)** The microtubule has made contact with the cortical Kar9–GFP spot in the bud, and the SPB has moved towards the neck. **(d)** The microtubule has separated from the Kar9–GFP spot. During this time, SPB movement towards the bud ceases. **(e)** The microtubule is recaptured by Kar9–GFP, and SPB migration continues



towards the bud. **(f)** The nucleus is positioned at the neck with the microtubule extending into the bud. Elapsed time (min) is shown. These images were generated using a Delta-Vision imaging workstation. **(g)** The distance between the Kar9–GFP spot and the SPB

was measured for each frame in the time lapse and plotted against time. Each point displaying an intersection or separation of the Kar9–GFP spot and the microtubule was scored by observing individual optical sections. See Supplementary movie 7.

microtubules lost contact with the Kar9p spot (Figure 6d), then resumed once contact was re-established (Figure 6e).

The distance between the SPB and the Kar9–GFP spot within the bud is plotted in Figure 6g. Microtubule–Kar9p contacts were scored in frames where the labeled microtubule terminated in a region occupied by a Kar9–GFP spot. Periods with the most dramatic nuclear movements towards the bud (~20 minutes and ~30 minutes) coincided with intersection of the Kar9–GFP spot and microtubule. In the cell shown, the apparent microtubule–Kar9p attachment remained stable after the nucleus had reached the neck. The SPB did not proceed into the bud, although colocalization of Kar9–GFP and microtubules was evident (Figure 6g, ~40–60 minutes).

Positioning the nucleus at the neck in vegetative cells is analogous to nuclear migration to the tip of the mating projection [49]. Kar9–GFP localizes to the mating projection tip, and is required for nuclear orientation and migration during the mating process [5,9]. We observed nuclear migration towards the mating projection tip of α -factor-treated cells expressing both dynein–GFP and Kar9–GFP. In cells entering the mating pathway, nuclei rotate opposite to the direction of microtubule growth until the mating projection tip is located (similar to nuclear movement in unbudded vegetative cells). Microtubules formed persistent connections with the Kar9–GFP spot, and the nucleus migrated toward the mating projection (Figure 7a–f) at $0.32 \pm 0.13 \mu\text{m}/\text{minute}$ ($n = 11$), which was similar to the velocity of nuclear migration to cortical Kar9p in vegetative cells.

The distance from the SPB to the mating projection tip is plotted in Figure 7g, which demonstrates the movement of the SPB towards the mating projection base. After the microtubule had oriented towards the mating projection

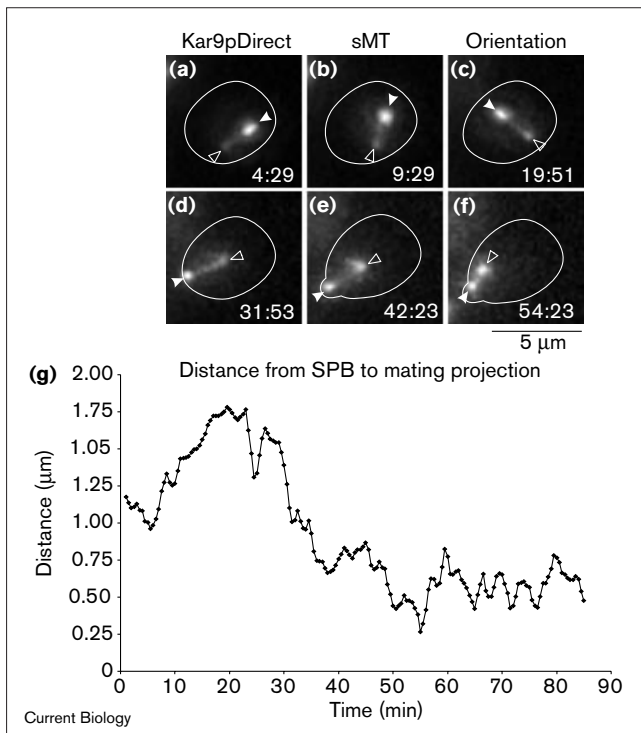
(27–30 minutes), nuclear movement towards the mating projection coincided with microtubule depolymerization [49]. After the nucleus was positioned at the base of the mating projection, the distance between the SPB and the mating projection lengthened and shortened over the ensuing 45 minutes. SPB movement was facilitated by microtubule growth and shrinkage while maintaining an interaction with the Kar9–GFP spot. Thus, Kar9p–microtubule interactions facilitate nuclear migration in both vegetative and mating cycles.

Directed movement to the neck is differentiated from steady state, oscillatory nuclear movements in vegetative (Figure 6g) and mating (Figure 7g) cells. Directional transport of the nucleus towards the neck is observed in Figure 6 (~20–40 minutes) and Figure 7 (~25–55 minutes). During directed nuclear movement to the neck, $62\% \pm 20$ ($n = 6$) of time points showed an intersection between Kar9–GFP and microtubules, $69\% \pm 9.4$ ($n = 5$) of which resulted in directed movement of the nucleus towards the neck. Thus, not every microtubule intersection with a Kar9–GFP spot results in directed nuclear movement. Following nuclear congression, oscillatory movements maintained a steady state positioning of the nucleus adjacent to the neck or mating projection until either anaphase or cell fusion occurred (Figure 6, ~40–65 minutes; and Figure 7, ~55–85 minutes). The persistence of the association of microtubules to Kar9–GFP spots increased to $75\% \pm 28$ ($n = 4$) of these time points, but did not result in directed movements past the neck.

Discussion

Kar9p, Bud6p, Bni1p and Bim1p together constitute an early pathway to position the nucleus at the bud neck before the onset of anaphase. We observed that Kar9p was present throughout the cell cycle in dynamic equilibrium between microtubules and sites of polarized growth. Its

Figure 7



Kar9p directs microtubule orientation towards the mating projection. (a–f) Selected time-lapse images of a cell expressing both Kar9–GFP and dynein–GFP in the presence of α -factor. Dynein–GFP decorated the SPB (open arrowhead) and the microtubule, while Kar9–GFP labeled the plus-end of the microtubule (solid arrowhead). (a–d) The microtubule rotated approximately 180° counter-clockwise to orient the plus-end of the microtubule at the tip of the mating projection. Rotation was complete at the 26:53 time point. (d–f) Following microtubule orientation, microtubule shortening moved the SPB to the base of the mating projection. Elapsed time (in min) is shown. (g) The distance between the SPB and the mating projection tip was measured for each frame in the time-lapse series and plotted against time. Microtubule interactions with the Kar9–GFP spot were retained throughout the time-lapse series.

association with microtubules was susceptible to nocodazole treatment and required *BIMI* (Figure 2g–j, Table 1) [5,32,33,39]. Localization of Kar9p at the bud cortex was sensitive to treatment with latrunculin-A and was dependent on actin, *BNI1* and *BUD6* (Figure 2g–j, Table 1) [3]. Kar9p has not been shown, either biochemically or genetically, to associate simultaneously with microtubules and actin filaments. Time-lapse images of live cells coexpressing Kar9–GFP and dynein–GFP demonstrated that both proteins co-localized at the bud cortex, and correlated nuclear movements towards the bud with Kar9p–microtubule interactions in both vegetative and mating cells (see below).

Kar9–GFP was observed primarily as a cortical spot that was motile within the bud and not confined to the bud tip (Table 1, columns b–d). The asymmetric distribution of

Kar9p was established through an actomyosin transport system. Directional transport towards the bud was provided by two type V myosins, encoded by *MYO2* [52] and *MYO4* [53]. Myo2p supports polarized secretion [20], whereas the only known cargo for Myo4p is *ASH1* mRNA. In the absence of Myo2p, but not Myo4p, Kar9–GFP spots were present within the mother cell domain (Figure 3), demonstrating *MYO2*-dependent transport of Kar9p [34]. Single particle tracking of Kar9–GFP allowed us to obtain *in vivo* velocities for Myo2p-based motility. Kar9p followed a direct path towards the neck at approximately 1.52 μm/second (Figure 4), which is faster than *in vivo* Myo4p transport of *ASH1* mRNA (0.2–0.4 μm/second) [25] and *in vitro* motility assays using chick brain myosin V (0.2–0.4 μm/second) [54].

Directional transport by Myo2p requires actin cables polarized with their growing ends towards the bud [20]. Tropomyosin, an actin filament binding protein, is required to maintain actin cables, but does not effect the integrity of the actin patches [19]. Aberrant Kar9–GFP localization in the absence of tropomyosin implicates actin cables in Kar9p delivery to the bud, and further supports a Myo2p-dependent, actomyosin delivery system for Kar9p. Two independent spots of Kar9–GFP traveled approximately 3.5 μm within the same 0.3 μm-wide path through the cell between mother and bud, separated by about 2.6 seconds (Figure 4f). The similar trajectories followed by both Kar9p particles indicate that actin filaments persist long enough to allow transport of multiple particles on a single filament. Whether individual cables provide the substrate for different class V myosins (*ASH1* mRNA via Myo4p; Kar9p via Myo2p), or dedicated cables exist for one type of cargo (Kar9p versus vesicular traffic) remains to be determined.

In the absence of Kar9p, microtubules are delayed in detecting the bud site by approximately 45 minutes, potentially leading to off-axis microtubule spindles and the observed production of binucleated cells [5]. While Kar9p, *ASH1* mRNA, and Bud6p are localized similarly in budded cells, only Kar9p does not localize to the incipient bud site. Instead, Kar9–GFP was observed on microtubules and at the spindle pole body prior to bud emergence (Figure 2e,f). Kar9–GFP-decorated microtubules became oriented towards the bud site prior to bud emergence (Figure 5), and towards the mating projection tip (Figure 7a–f). Thus, putative transport of Kar9p-decorated microtubules along polarized actin fibers towards the bud would provide a ‘facilitated’ microtubule search and capture mechanism contributing to the fidelity of nuclear migration.

Once microtubules penetrate the bud, Kar9p at the bud cortex can provide a microtubule anchorage site [3,5]. Dynein–GFP-labeled microtubules reaching the bud cortex or the mating projection terminated at spots of Kar9–GFP

(Figure 6c,e,f, Figure 7d,f). Microtubule interactions with Kar9p in the bud lasted between 2–3 minutes, suggesting that microtubules transiently attach at Kar9p cortical sites. Following microtubule capture within the bud, the nucleus migrates subjacent to the neck and remains there until anaphase onset (Figure 6) [4,51]. Similarly, nuclear congression to the mating projection tip was accompanied by a persistent association of microtubules with a Kar9–GFP spot (Figure 7).

Nuclear movements towards and away from the bud or mating projection were coupled with shortening and lengthening of the microtubules connecting the spindle pole body to the Kar9p spot at the cortex (Figures 6a–f and 7a–f). The motor protein Kip3p is thought to stimulate microtubule disassembly, and is presumed to function in association with Kar9p, as *kip3p dhc1* and *kar9 dhc1* double mutants are lethal [8,27,30]. Kip3p at the microtubule–Kar9p junction could stimulate microtubule shortening, providing the underlying mechanism for nuclear migration. Kip3p has recently been shown to facilitate nuclear movement to the bud neck [4,8,27,30], but pulling forces exerted by Kip3p and associated proteins in the ‘early’ nuclear orientation pathway appear to be too weak to move the nucleus through the narrow neck [4]. Thus, a cooperative mechanism between Kar9p and Myo2p as well as Kar9p and Kip3p facilitates pre-anaphase nuclear positioning at the neck but not beyond. Subsequently, the late nuclear-orientation pathway, including the microtubule-based motor, dynein and associated proteins, supports translocation of the daughter nucleus into the bud in conjunction with spindle elongation for the successful completion of mitosis.

Materials and methods

Velocity measurements, microscopy and image processing

Kar9p velocity measurements were obtained measuring the point-to-point movements of Kar9–GFP spots. Kar9–GFP spots were tracked using the ‘Track Points’ function of the Metamorph (Universal Imaging Corporation) software package. The distance of spot movements at 30 sec (Figures 1,6) or 0.3 sec (Figure 4) intervals provided instantaneous velocities representing a minimal speed at each time point, and averaged over time. Only movements between sequential images were considered for velocity measurements. Because the spots frequently changed direction between long time points, continuous velocities could not be measured.

Microscopy and digital imaging, including optical sectioning, was performed as described in [37]. Five optical sections were taken at 0.75 μm increments through the cell for a total of 3.0 μm per time point. Rapid imaging rates of cells at 3 frames per second included only a single optical section. The central optical section including both a transmitted light and an epifluorescent (GFP) image was focused at the cell neck. Images were captured using a Hamamatsu Orca II (model C4742-98) CCD camera mounted on a Nikon Eclipse E600FN using 100 \times 1.4 NA Plan Achromat objective with 1 \times magnification to the camera. Image taken at elevated temperature for analysis of temperature sensitive strains used a Nikon Eclipse TE300 inverted microscope with a phase contrast 100 \times 1.4 NA Plan Achromat objective with 1 \times magnification to a Hamamatsu Orca (model C4742-95) camera. The inverted microscope stage was heated to 35°C over 25–30 min using a Nevtek air steam stage

incubator (model ASI400). The Metamorph software package for Windows was used for microscope automation, image acquisition and image analysis. Images for publication were manipulated for scaling, size, resolution (300 dpi) and arrangement with Windows versions of Adobe Photoshop and Corel Draw.

The ‘Kymograph’ function of Metamorph software was used to create a cross-sectional display of pixel intensity values along a linear region (line width of 5 pixels = 0.3 μm) for each image of a time-lapse series (Figure 4e) The ‘Linescan’ function of Metamorph provided numerical values and a graph representing the grayscale pixel values along a linear region for a single image plane from a time-lapse series. Three-dimensional reconstructions of cells were generated using the ‘3D Reconstruction’ function of Metamorph set for either full circle or shallow tile horizontal reconstructions with a Z distance of 1 μm per image for the five images of each optical section series. The ‘Stereographic Views’ function of Metamorph generated side-by-side images to view the three-dimensional reconstruction in printed format, with a 10° rotation between images. Images acquired using a DeltaVision (Applied Precision) deconvolution microscope were used in Figure 6. Briefly, using a 100X 1.4 NA Plan Apo lens on a Nikon TE200 inverted microscope, z-series consisting of 9 200 ms fluorescent (using a HQ-FITC filter set, Chroma Filters) exposures (0.3 μm step size) were acquired at 30 sec intervals. The z-series time lapse was then deconvolved using DeltaVision software and is presented as a maximum projection.

Supplementary material

Supplementary material including additional methodological detail is available at <http://current-biology.com/supmat/supmatin.htm>.

Acknowledgements

We thank John Pringle, Katja Schwartz and Rita Miller for strains and plasmids; Ted Salmon for imaging advice and critical reading of the manuscript; Chad Pearson for critical reading of the manuscript; and Susan Whitfield, Jennifer Stemple and Molly Hays for technical assistance. This work is supported by National Institutes of Health grant GM32238 to K.B.

References

1. Heil-Chapdelaine RA, Adames NR, Cooper JA: **Formin’ the connection between microtubules and the cell cortex.** *J Cell Biol* 1999, **144**:809-811.
2. Lee L, Klee SK, Evangelista M, Bonne C, Pellman D: **Control of mitotic spindle position by the *Saccharomyces cerevisiae* formin Bni1p.** *J Cell Biol* 1999, **144**:947-961.
3. Miller R, Matheos D, Rose M: **The cortical localization of the microtubule orientation protein, Kar9p, is dependent upon actin and proteins required for polarization.** *J Cell Biol* 1999, **144**:963-975.
4. Yeh E, Yang C, Chin E, Maddox P, Salmon ED, Lew DJ, *et al.*: **Dynamic positioning of mitotic spindles in yeast: role of microtubule motors and cortical determinants.** *Mol Biol Cell* 2000, **11**:1-13.
5. Miller RK, Rose MD: **Kar9p is a novel cortical protein required for cytoplasmic microtubule orientation in yeast.** *J Cell Biol* 1998, **140**:377-390.
6. Eshel D, Urrestarazu LA, Vissers S, Jauniaux JC, van Vliet-Reedijk JC, Planta RJ, *et al.*: **Cytoplasmic dynein is required for normal nuclear segregation in yeast.** *Proc Natl Acad Sci USA* 1993, **90**:11172-11176.
7. Li YY, Yeh E, Hays T, Bloom K: **Disruption of mitotic spindle orientation in a yeast dynein mutant.** *Proc Natl Acad Sci USA* 1993, **90**:10096-10100.
8. Miller RK, Heller KK, Rose MD: **The kinesin-related proteins, Kip2p and Kip3p, function differently in nuclear migration in yeast.** *Mol Biol Cell* 1998, **9**:2051-2068.
9. Kurihara LJ, Beh CT, Latterich M, Schekman R, Rose MD: **Nuclear congression and membrane fusion: two distinct events in the yeast karyogamy pathway.** *J Cell Biol* 1994, **126**:911-923.
10. Evangelista M, Blundell K, Longtine MS, Chow CJ, Adames N, Pringle JR, *et al.*: **Bni1p, a yeast formin linking Cdc42p and the actin cytoskeleton during polarized morphogenesis.** *Science* 1997, **276**:118-122.

11. Amberg DC, Zahner JE, Mulholland JW, Pringle JR, Botstein D: **Aip3p/Bud6p, a yeast actin-interacting protein that is involved in morphogenesis and the selection of bipolar budding sites.** *Mol Biol Cell* 1997, **8**:729-753.
12. Fujiwara T, Tanaka K, Mino A, Kikyo M, Takashi K, Shimizu K, et al.: **Rho1p-Bni1p-Spa2p interactions: implication in localization of Bni1p at the bud site and regulation of the actin cytoskeleton in *Saccharomyces cerevisiae*.** *Mol Biol Cell* 1998, **9**:1221-1233.
13. Palmer RE, Sullivan DS, Huffaker T, Koshland D: **Role of astral microtubules and actin in spindle orientation and migration in the budding yeast, *Saccharomyces cerevisiae*.** *J Cell Biol* 1992, **119**:583-593.
14. Theesfeld CL, Irazoqui JE, Bloom K, Lew DJ: **The role of actin in spindle orientation changes during the *Saccharomyces cerevisiae* cell cycle.** *J Cell Biol* 1999, **146**:1019-1032.
15. Wang T, Bretscher A: **Mutations synthetically lethal with *tpm1Δ* lie in genes involved in morphogenesis.** *Genetics* 1997, **147**:1595-1607.
16. Yang CH, Snyder M: **The nuclear-mitotic apparatus protein is important in the establishment and maintenance of the bipolar mitotic spindle apparatus.** *Mol Biol Cell* 1992, **3**:1259-1267.
17. Adams AEM, Botstein D, Drubin DG: **Requirement of yeast fimbrin for actin organization and morphogenesis *in vivo*.** *Nature* 1991, **354**:404-408.
18. Kopecká M, Gabriel M: **The aberrant positioning of nuclei and the microtubular cytoskeleton in *Saccharomyces cerevisiae* due to improper actin function.** *Microbiology* 1998, **144**:1783-1797.
19. Pruyne DW, Schott DH, Bretscher A: **Tropomyosin-containing actin cables direct the Myo2p-dependent polarized delivery of secretory vesicles in budding yeast.** *J Cell Biol* 1998, **143**:1931-1945.
20. Karpova TS, Reck-Peterson SL, Elkind NB, Mooseker MS, Novick PJ, Cooper JA: **Role of actin and Myo2p in polarized secretion and growth of *Saccharomyces cerevisiae*.** *Mol Biol Cell* 2000, **11**:1727-1737.
21. Jin H, Amberg DC: **The secretory pathway mediates localization of the cell polarity regulator Aip3p/Bud6p.** *Mol Biol Cell* 2000, **11**:647-661.
22. Long RM, Singer RH, Meng X, Gonzalez I, Nasmyth K, Jansen R-P: **Mating type switching in yeast controlled by asymmetric localization of *ASH1* mRNA.** *Science* 1997, **277**:383-387.
23. Takizawa PA, Sil A, Swedlow JR, Herskowitz I, Vale RD: **Actin-dependent localization of an RNA encoding a cell-fate determinant in yeast.** *Nature* 1997, **389**:90-93.
24. Beach DL, Salmon ED, Bloom K: **Localization and anchoring of mRNA in budding yeast.** *Curr Biol* 1999, **9**:569-578.
25. Bertrand E, Chartrand P, Schaefer M, Shenoy SM, Singer RH, Long RM: **Localization of *ASH1* mRNA particles in living yeast.** *Mol Cell* 1998, **2**:437-445.
26. Jansen RP, Dowzer C, Michaelis C, Galova M, Nasmyth K: **Mother cell-specific *HO* expression in budding yeast depends on the unconventional myosin Myo4p and other cytoplasmic proteins.** *Cell* 1996, **84**:687-697.
27. DeZwaan TM, Ellingson E, Pellman D, Roof DM: **Kinesin-related KIP3 of *Saccharomyces cerevisiae* is required for a distinct step in nuclear migration.** *J Cell Biol* 1997, **138**:1023-1040.
28. Straight AF, Sedat JW, Murray AW: **Time-lapse microscopy reveals unique roles for kinesins during anaphase in budding yeast.** *J Cell Biol* 1998, **143**:687-694.
29. Schwartz K, Richards K, Botstein D: **BIM1 encodes a microtubule-binding protein in yeast.** *Mol Biol Cell* 1997, **8**:2677-2691.
30. Cottingham FR, Hoyt MA: **Mitotic spindle positioning in *Saccharomyces cerevisiae* is accomplished by antagonistically acting microtubule motor proteins.** *J Cell Biol* 1997, **138**:1041-1053.
31. Tirnauer JS, O'Toole EO, Berrueta L, Bierer BE, Pellman D: **Yeast Bim1p promotes the G1-specific dynamics of microtubules.** *J Cell Biol* 1999, **145**:993-1007.
32. Korinek WS, Copeland MJ, Chaudhuri A, Chant J: **Molecular linkage underlying microtubule orientation toward cortical sites in yeast.** *Science* 2000, **287**:2257-2259.
33. Lee L, Tirnauer JS, Li J, Schuyler SC, Liu JY, Pellman D: **Positioning of the mitotic spindle by a cortical-microtubule capture mechanism.** *Science* 2000, **287**:2260-2262.
34. Yin H, Pruyne D, Huffaker TC, Bretscher A: **Myosin V orients the mitotic spindle in yeast.** *Nature* 2000, **406**:1013-1015.
35. Waddle JA, Karpova TS, Waterston RH, Cooper JA: **Movement of cortical actin patches in yeast.** *J Cell Biol* 1996, **132**:861-870.
36. Marshall WF, Straight A, Marko JF, Swedlow J, Dernberg A, Belmont L, et al.: **Interphase chromosomes undergo constrained diffusional motion in living cells.** *Curr Biol* 1997, **7**:930-939.
37. Shaw SL, Yeh E, Maddox P, Salmon ED, Bloom K: **Astral microtubule dynamics in yeast: a microtubule-based searching mechanism for spindle orientation and nuclear migration into the bud.** *J Cell Biol* 1997, **139**:985-994.
38. Straight AF, Marshall WF, Murray AW: **Mitosis in living budding yeast: anaphase A but no metaphase plate.** *Science* 1997, **277**:574-578.
39. Miller RK, Cheng S-C, Rose MD: **Bim1p/Yeb1p mediates the Kar9p-dependent cortical attachment of cytoplasmic microtubules.** *Mol Biol Cell* 2000, **11**:2949-2959.
40. Munchow S, Sauter C, Jansen RP: **Association of the class V myosin Myo4p with a localized messenger RNA in budding yeast depends on She proteins.** *J Cell Sci* 1999, **112**:1511-1518.
41. Lillie SH, Brown SS: **Suppression of a myosin defect by a kinesin-related gene.** *Nature* 1992, **356**:358-361.
42. Ayscough KR, Stryker J, Pokala N, Sanders M, Crews P, Drubin DG: **High rates of actin filament turnover in budding yeast and roles for actin in establishment and maintenance of cell polarity revealed using the actin inhibitor latrunculin-A.** *J Cell Biol* 1997, **137**:399-416.
43. Adams AEM, Pringle JR: **Relationship of actin and tubulin distribution to bud growth in wild-type and morphogenetic-mutant *Saccharomyces cerevisiae*.** *J Cell Biol* 1984, **98**:934-945.
44. Kilmartin JV, Adams EM: **Structural rearrangements of tubulin and actin during the cell cycle of the yeast *Saccharomyces*.** *J Cell Biol* 1984, **98**:922-933.
45. Li R, Zheng Y, Drubin DG: **Regulation of cortical actin cytoskeleton assembly during polarized cell growth in budding yeast.** *J Cell Biol* 1995, **128**:599-615.
46. Carminati JL, Stearns T: **Microtubules orient the mitotic spindle in yeast through dynein-dependent interactions with the cell cortex.** *J Cell Biol* 1997, **138**:629-641.
47. Goode BL, Wong JJ, Butty A-C, Peter M, McCormack AL, Yates JR, et al.: **Coronin promotes the rapid assembly and cross-linking of actin filaments and may link the actin and microtubule cytoskeletons in yeast.** *J Cell Biol* 1999, **144**:83-98.
48. Goode BL, Drubin DG, Barnes G: **Functional cooperation between the microtubule and actin cytoskeletons.** *Curr Opin Cell Biol* 2000, **12**:63-71.
49. Maddox P, Chin E, Mallavarapu A, Yeh E, Salmon ED, Bloom K: **Microtubule dynamics from mating through the first zygotic division in the budding yeast *Saccharomyces cerevisiae*.** *J Cell Biol* 1999, **144**:977-987.
50. Heil-Chapdelaine RA, Tran NK, Cooper JA: **The role of *Saccharomyces cerevisiae* coronin in the actin and microtubule cytoskeletons.** *Curr Biol* 1998, **8**:1281-1284.
51. Adames NR, Cooper JA: **Microtubule interactions with the cell cortex causing nuclear movements in *Saccharomyces cerevisiae*.** *J Cell Biol* 2000, **149**:1-13.
52. Johnston GC, Prendergast JA, Singer RA: **The *Saccharomyces cerevisiae* MYO2 gene encodes an essential myosin for vectorial transport of vesicles.** *J Cell Biol* 1991, **113**:539-551.
53. Haarer BK, Petzold A, Lillie SH, Brown SS: **Identification of MYO4, a second class V myosin gene in yeast.** *J Cell Sci* 1994, **107**:1055-1064.
54. Cheney RE, O'Shea, Heuser MK, Coelho MV, Wolenski JS, Espreafico EM, et al.: **Brain myosin-V is a two-headed unconventional myosin with motor activity.** *Cell* 1993, **75**:13-23.

Because *Current Biology* operates a 'Continuous Publication System' for Research Papers, this paper has been published on the internet before being printed. The paper can be accessed from <http://biomednet.com/cbiology/cub>